Fluid-Structure Interaction Analysis Applied to Thermal Barrier Coated Cooled Rocket Thrust Chambers with Subsequent Local Investigation of Delamination Phenomena

Daniel S.C. Kowollik, Peter Horst and Matthias C. Haupt
Institute of Aircraft Design and Lightweight Structures
TU Braunschweig
Herrmann-Blenk-Str. 35, 38106 Braunschweig, Germany

Abstract

The aim of this work is to investigate numerically thermal barrier coating (TBC) systems applied to realistic rocket thrust chamber conditions. A global full parametric 3D modelling approach for cooled rocket thrust chambers is presented to be able to simulate the fluid structure interaction (FSI) phenomena involved. In a subsequent analysis step realistic mechanical and thermal boundary conditions are extracted from critical design regions of the global model and applied to a local finite element model to analyse possible TBC delaminations by means of a Fracture Mechanics (FM) approach.

1. Introduction

The wall of modern liquid rocket engines is exposed to extreme thermal loadings. In current designs high aspect ratio cooling channels are milled in the copper liner, whereas the chamber wall is approximately 1 mm thick. This setup is kept intact only for a few engine cycles. A protection of the thin copper cooling structure is a promising strategy to enhance thrust chamber life. Thermal barrier coatings are widely used in applications at elevated temperatures, e.g. automotive, gas turbines and aero-engines. The transfer of TBC systems to rocket applications offers great potential to reduce coolant temperature and pressure loss in the cooling cycle based on the reduction of heat flux acting on the hot gas surface inside the combustion chamber. A careful design is necessary to cope with the transient boundary conditions, under which TBCs tend to spall, delaminate and crack.

The response of the cooling channel can only be addressed through an adequate prediction of the in-service conditions. Chemical reactions during the combustion process, fluid flow in the thrust chamber and cooling channels, heat transfer between the involved domains and the thermomechanical coupling in the structure make up a complex system. The thermal and pressure loads generated by the hot gas and the cooling channel flow are essential for the prediction of the cooling channel response. Computer resources in the past were limited to the application of simplified models for coupled simulations. In [1] the thermal interaction between a 2D structural model and a straight 3D cooling channel segment is analysed. The interaction with the hot gas side is neglected, whereas experimental data of [2] serve as boundary condition. This simplified model is extended by a thermomechanical coupling strategy in [3]. A 3D coupled heat transfer analysis is presented by Liu et al. in [4], where the hot gas and cooling channel structure are modelled by a finite volume scheme. The cooling channel flow is included by a 1D approach. Current simulation strategies were presented by Knab et al. in [5], where a coupled heat transfer simulation is performed between the hot gas side and the coolant flow. The hot gas side is modelled by an axisymmetric multi-phase Navier-Stokes solver, whereas the cooling channel flow and the structure are analysed by a 3D conjugate heat transfer model.

This paper extends the previous studies by accounting for the full thermal and mechanical interactions between the hot flow field and the structure by applying TBC systems to a parametric 3D modelling approach, which is presented. A subsequent local investigation with applied boundary conditions of the global analyses gives first insight in the loading conditions acting on macroscopic delaminations being located at the critical throat region of the thrust chamber.

2. Coupled simulation approach

Analysing cooled rocket thrust chambers demands for the consideration of thermal and mechanical fluid-structure interaction. The developed simulation environment ifls covers both physical couplings in a partitioned approach using individual codes for the involved subdomains fluid and structure. A detailed description of *ifls* can be taken from [6]. Validation studies of coupled problems analysed by different individual code combinations are presented in [6, 7, 8].

The two coupling aspects that need to be considered applying a partioned approach for a steady state analysis are the data transfer of the variables to be coupled through nonconforming surface discretizations and the solution of the equilibrium equations.

2.1 Nonconforming spacial discretization at the interface

Data transfer between nonconforming surface discretizations at the coupling interface Γ_c can be achieved in a conservative manner by applying a weak formulation to the continuity conditions [9], where the variations of the involved state variables ϕ (temperatures T and deflections u) are weighted by Lagrange multipliers λ_ϕ as follows:

$$\int_{\Gamma_c} \lambda_T \left(T^{(s)} - T^{(f)} \right) \mathrm{d}\Gamma \quad , \quad \int_{\Gamma_c} \lambda_u \left(u^{(s)} - u^{(f)} \right) \mathrm{d}\Gamma \quad . \tag{1}$$

The indices (s) and (f) represent the fluid and the structural domains. In the discrete form equation 1 results in the matrix system $\phi^{(f)}|_\Gamma = \mathbf{H}\,\phi^{(s)}|_\Gamma$ by using shape functions for the Lagrange multipliers and for the individual domain discretizations fluid and structure at the interface. The transformation matrix $\mathbf{H}$ can be used in its tranposed form in order to guarantee conservation of energy, if the consistent mechanical and thermal discrete fluxes are transferred normal to the interface: $\phi^{(f)}_{,\mathbf{n}}|_\Gamma = \mathbf{H}^{\mathrm{T}}\,\phi^{(s)}_{,\mathbf{n}}|_\Gamma$.

If the mesh discretization does not differ significantly between the individual domains, the Dirac delta functions applied at the fluid interface nodes are the standard choice for the shape functions of the Lagrange multiplier. Strong discretization mismatch will result in unphysical load peaks, which can be alleviated by a locally more accurate approach, where the fluid shape functions are used for the Lagrange multiplier leading to an approach comparable to the Mortar-technique, see [10].

2.2 Solution of the partitioned formulation

The solution of the coupled problem is obtained by the Dirichlet-Neumann iteration. Formulating the Dirichlet problem in terms of a Schur complement one defines symbolically the fluid operator $\mathcal{F}$ as follows: $\mathcal{F}\,\phi^{(f)}|_\Gamma = \phi^{(f)}_{,\mathbf{n}}|_\Gamma$, where ϕ represents the state variables and $\phi_{,\mathbf{n}}$ the flux at the coupling interface Γ. The inverse Schur complement is formulated for the structural problem, consequently the Neumann problem is solved:

$$\phi^{(s)}_{,\mathbf{n}}|_\Gamma = \mathcal{S}^{-1}\,\phi^{(s)}|_\Gamma \;\longleftrightarrow\; \mathcal{S}\,\phi^{(s)}|_\Gamma = \phi^{(s)}_{,\mathbf{n}}|_\Gamma \,. \tag{2}$$

For the classical Dirichlet-Neumann iteration a relaxation scheme is applied to the state variables in each steady state iteration step as follows:

$$\phi_{k+1} = (1-\omega)\,\phi_k + \omega\,\mathcal{S}^{-1}\,\mathcal{F}\,\phi_k \,, \tag{3}$$

with the relaxation parameter ω. For the coupled problem in the present work a choice of a fixed $\omega = 0.8$ was sufficient to achieve a noticeable reduction of the residual during the fixed point iteration.

3. Parametrized thrust chamber modelling approach

3D FSI analyses of cooled rocket thrust chambers are computationally expensive. Computational reduction can be achieved if symmetry conditions are used, consequently the assumption of the present parametric approach is to model half of a cooling channel segment for the combustion chamber cooling circuit. The hot gas is modelled with periodic boundary conditions, which is shown in figure 1(a), where the coupling surfaces are defined. The data transfer between the hot gas and structural domain is achieved through an additional coupling surface $\Gamma_{s,hf,full}$, where the state and flux variables are mirrored to satisfy integrity of the applied boundary conditions in each iteration step. Accounting for all

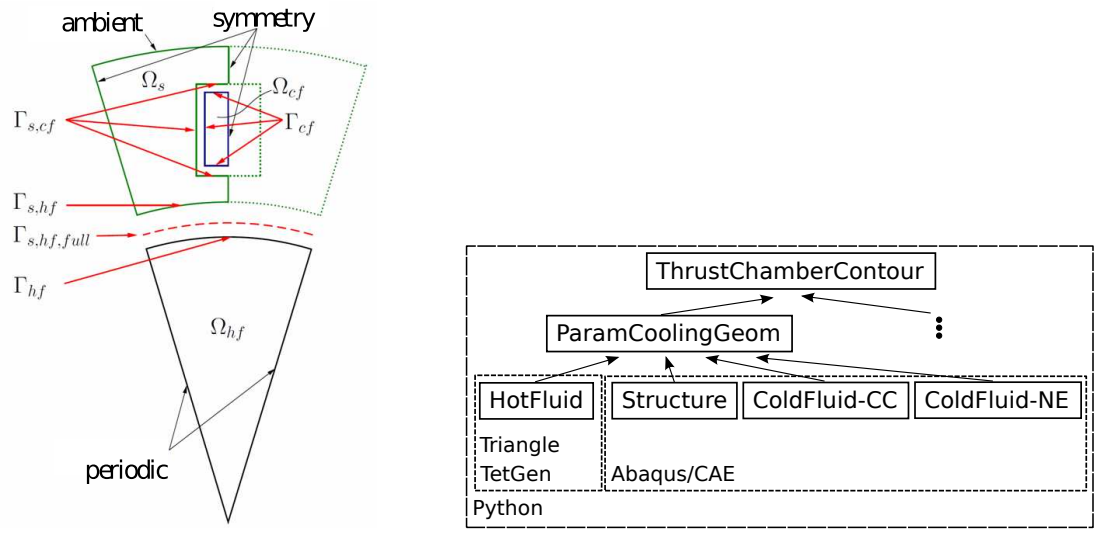

(a) Definition of coupling surfaces. (b) Software concept.

Figure 1: Parametrized modelling aspects of cooled rocket engines.

symmetry conditions in the different computational domains allows the simulation of the 3D state by the assumption of periodic repetition.

A software concept for parametrized modelling of thrust chamber designs and cooling channel setups was developed and is shown schematically in figure 1(b). The parametrization reaches from the thrust chamber contour and cooling channel design to the CAD modelling and finally to the grid generation of the hot gas, structure and cooling channel flow field. The software architecture uses the Python interface to the preprocessor Abaqus/CAE. Python scripting allows an object oriented modular and reusable framework for the different components of the parametrized models. Additional software packages like Triangle [11] and TetGen [12] are used to discretize the unstructured part of the hybrid hot gas grid.

The class definition of *ThrustChamberContour* describes the complete rocket engine contour of figure 2 (left), where the nozzle is designed with the thrust optimized parabola (TOP) from Rao [13]. The TOP nozzle can be described by five independent variables r_{td}, θ_n, L, r_e and θ_e. The angles θ_n and θ_e are evaluated through a bivariate spline whose input data was taken from Rao [13]. Even modern nozzles like the Vulcain and SSME nozzle can be studied by means of a parabolic contour [14].

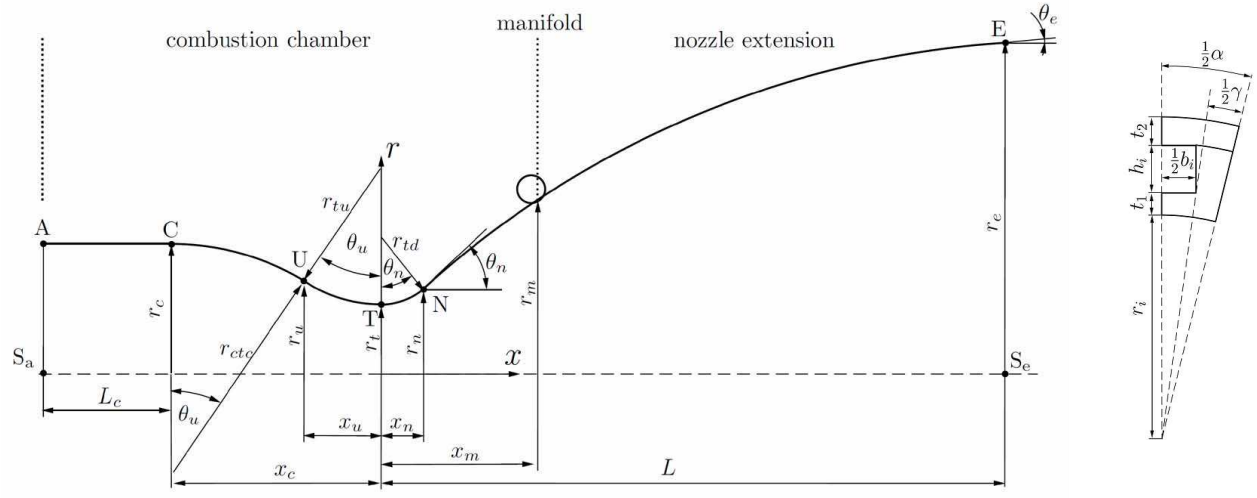

Figure 2: Parametrized model: thrust chamber contour (left); cooling channel cross section (right).

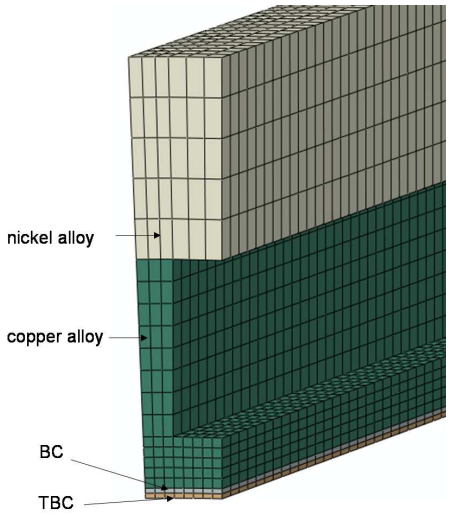

Figure 3: Close view of the material setup of the parametrized global structural model.

The derived class *ParamCoolingGeom* accounts for the chosen cooling circuit cross section definition shown on the right of figure 2. For the present cooling channel setup classes are derived for the different computational domains, which implement the parametrized CAD and grid models. In this study the analysed subscale thrust chamber consists of three domains structure, hot gas and the two cooling curcuits, one in the combustion chamber region and one in the nozzle extension. For both cooling circuits a continously varying cooling channel geometry can be defined for the cross section sketched in figure 2 (right).

The structural model is able to account for TBC systems consisting of up to two individual materials, which can be seen in figure 3. The copper and nickel material is modelled via 8 node linear solid elements and the thin TBC system materials are accounted for via 8 node linear solid shell elements.

4. FSI analyses of thermal barrier coated cooled rocket thrust chambers

Extracted general parameters of a 40 kN LOX/H_2 subscale rocket thrust chamber defined by Astrium Space Transportation GmbH, Propulsion & Equipment serve as input for the parametrized modelling approach. The thrust chamber features 80 cooling channels in the combustion chamber and 160 cooling channels in the nozzle extension.

On the hot gas side a 3D steady RANS analysis using ideal gas law assuming finalized combustion is performed in each Dirichlet step of the static FSI analysis. For the fluid simulaton the DLR TAU-Code [16] is used, which is an unstructured RANS solver based on the finite volume method. Reservoir pressure inflow conditions were computed with the preliminary design tool RPA (Rocket Propulsion Analysis) [15] and served as inlet conditions for the DLR TAU-Code. The temperature niveau computed with RPA reaches $3,502\,\mathrm{K}$ at a pressure level of $9.35\,\mathrm{MPa}$. At the nozzle exit supersonic outlet conditions are applied, while an isothermal wall is defined at the coupling surface. The turbulent effects are modelled by the original version of the Spalart-Allmaras model implemented in the TAU-Code. The hybrid grid consists of 590,833 grid points, 686,535 tetrahedra and 785,686 prisms. The dimensionless $y+$ is adapted to a maximum of 0.57 at the thrust chamber throat. Figure 4 shows the typical mach number profile of a TOP nozzle, where compression waves are generated at the intersection of the downstream arc and the parabola contour. These compression waves coalesce in an internal shock. Comparisons to Östlund approve these flow phenomena [14].

The steady state heat transfer problem of the cooling channel structure is analysed with the ABAQUS FE software. The resultant heatflux of the hot gas simulation is transfered as boundary condition on the coupling surface. Constant film coefficients are assumed for the two coolant circuits, whereas the film coefficient of $h_{f,CC} = 150\,\mathrm{kW/(m^2\,K)}$ is applied for the combustion chamber circuit and $h_{f,NE} = 30\,\mathrm{kW/(m^2\,K)}$ is applied for the nozzle extension circuit. For both circuits the sink temperature is defined as $T = 40\,\mathrm{K}$. Radiation effects in the combustion chamber are not considered so far. Radiation to ambient is computed for the outside facing surface of the cooling channel structure.

The resultant temperature distribution together with the mechanical loads are used as boundary conditions for the static stress/displacement analysis. At the inlet deflections in the axial direction are suppressed. Symmetric deformation is guaranteed by applying zero deflection normal to the symmetry planes sketched in figure 1(a). The material

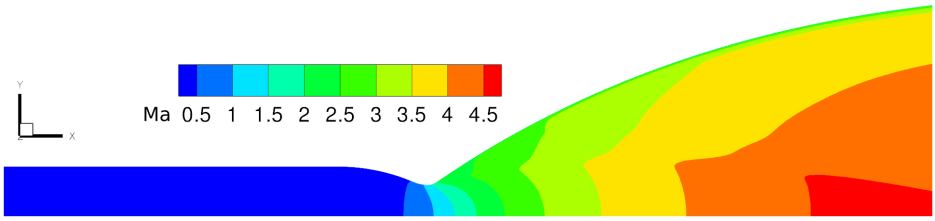

Figure 4: Mach number distribution at steady state of the coupled FSI analysis.

parameters of copper (substrate: CuCr1Zr), BC (bond coat: NiCrAlY) and TBC (top coat: zirconia) are taken from [17, 18, 19]. INCONEL alloy 600 [20] is used for the nickel jacket of the combustion chamber and the nozzle extension.

Two different coating systems are analysed by the above mentioned FSI analysis approach. The first applied TBC system can be reffered to as a conventional setup, where a 30μm bond coat and a 10μm top coat is defined on top of the hot gas wall. Figure 5 shows the converged temperature distribution of the structural domain. The high temperatures at the combustion chamber inlet can be explained by the assumption of finalized combustion at the inlet, where a homogenous inflow condition neglecting the typical injector head is applied.

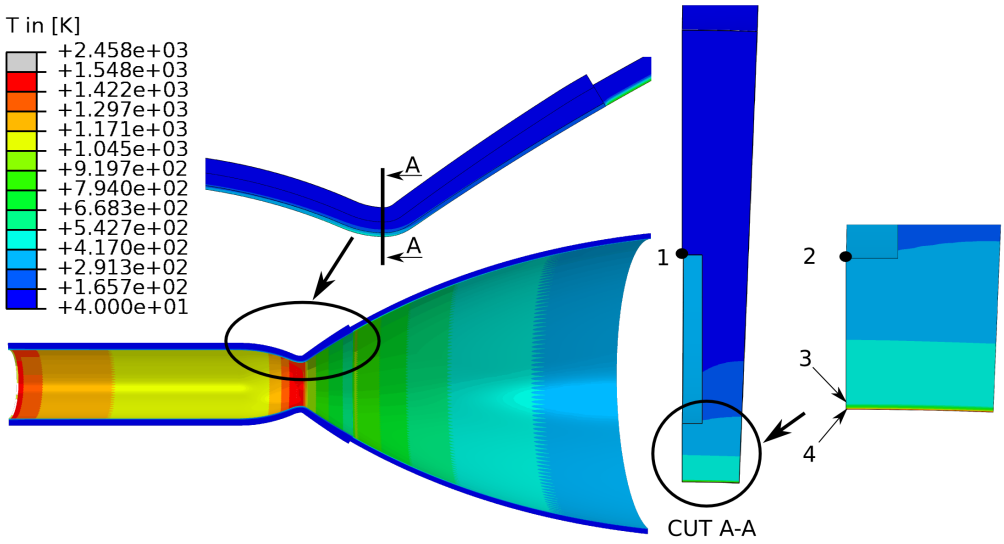

Figure 5: Temperature distribution for the BC = 30μm and TBC = 10μm thermal barrier coating at steady state.

Realistic physical conditions are met at the throat region, where the temperature peak reaches about 1516 K. The peak temperature is about 667 K higher compared to a conventional setup, where the copper substrate faces the hot gas directly.

Another small temperature peak can be identified in the nozzle extension just downstream of the manifold position. At this point a material and geometric cooling channel variation between the coated combustion chamber wall and the nozzle extension is located. The constant film coefficients in the upstream cooling curcuit are defined five times higher than in the downstream cooling cooling curcuit.

The cut view at the throat region shown on the right in figure 5 gives insights about the temperature distribution of the cooling channel cross section. The TBC system insulation results in a considerable temperature drop for the copper wall compared to conventional combustion chamber setups. Cross section temperature data for four different positions are defined in figure 5 and summarized in table 1. The maximum copper temperature is reached at position 3 with 476K for the first analysed TBC system.

For the second TBC system analysed in this study the top coat layer is omitted, where the bond coat layer is thickened up to 100μm. The insulation effect is compareable to the first analysed TBC system, which can be identified in table 1. Thicker one layer TBC systems allow cheaper manufacturing techniques like atmospheric plasma spraying, whereas the individual layers of the first analysed TBC system are too thin and would have to be manufactured for instance by vacuum plasma spraying. Another benefit of a one layer system is the reduction to only one remaining

Table 1: Temperature distribution at 4 points defined in figure 5 for two different TBC systems at steady state.

position	**BC = 30μm; TBC = 10μm**	**BC = 100μm**
1	50K	48K
2	324K	298K
3	497K	456K
4	1516K	1648K

interface problem which needs to be handled via optimal material compatibility between the copper substrate and the bond coat.

In addition to the thermal results, the global structural response of the steady state FSI analysis of the first TBC system is shown in figure 6. The effect of the global deformed state on the aerothermomechanical analysis is small compared to the strong influence of the thermal interactions.

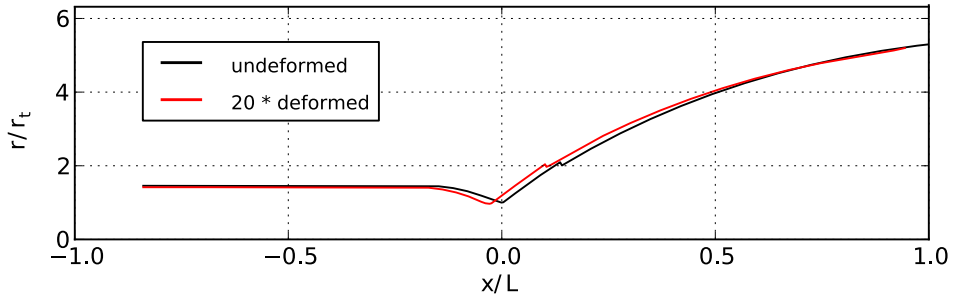

Figure 6: Deformed vs undeformed thrust chamber contour for the BC = 30μm and TBC = 10μm thermal barrier coating at steady state.

5. Local macro scale delamination modelling

Aside from erosion problems investigated by Quentmeyer et al. in [21] it was shown by Miller and Lowell in [22] that TBCs are prone to delamination at the interfaces and even ultimate failure by spallation phanomenon.

The failure phenomenon investigated here includes the effect of macroscopic delamination of TBC systems in rocket thrust chambers. Macro scale delamination modelling is well established in the field of fibrous composites, however, in the field of TBC systems applied to rocket thrust chambers macro scale delamination growth was not studied so far. This work focuses on the analyses of a Fracture Mechanics (FM) approach applied to TBC systems. For FM approaches an initial delamination must be present at which the crack tips are used to determine the fracture mechanical data. An assumed initial macro scale delamination may have an impact on the propagation behaviour, which must be studied in future.

Delamination propagation analysed by a FM approach follows directly from the energy release rate G computed by means of linear elastic fracture mechanics for a given loading compared to the critical value G_c. The fracture energy G_c is a material property and consequently independent of the loading. Several methods were proposed and validated to compute G or respectively its mode components G_I, G_{II} and G_{III}, e.g. J-Integral, Virtual Crack Extension, Virtual Crack Closure and Williams [23, 24, 25].

To gain first insides in the local loading behaviour of macro scale delaminations the Virtual Crack Closure Technique (VCCT) is a applied to study sensitivities for two different TBC systems mentioned above.

5.1 Virtual Crack Closure Technique

The Virtual Crack Closure Technique (VCCT) is a Fracture Mechanics FEM post-processing approach to compute mixed-mode energy release rates for each fracture mode component. The benefit of the VCCT is to be able to compute the mixed-mode energy release rates by using only one finite element analysis step. Other methods like the crack

closure method need two analysis steps, where the crack is physically extended or closed. In the following the theory and application of the VCCT to three-dimensional linear solid elements is summarized following Krüger [24].

The VCCT is based on two assumptions. The first assumption equals the crack closure method, where it is assumed that the energy needed to extend a crack from length a to the length $a + \Delta a$ is equal to the energy to close the crack by the same length Δa. The second assumption states that the crack tip configuration shown in figure 7(a) will not alter considerably if a crack is extended to the length $a + \Delta a$ or to $a + 2\Delta a$, meaning that the relative displacements between node Ll and node Ll^* behind the crack with length $a + \Delta a$ will be approximately the same displacement at node i, if node i is released and the crack is extended to the length $a + 2\Delta a$.

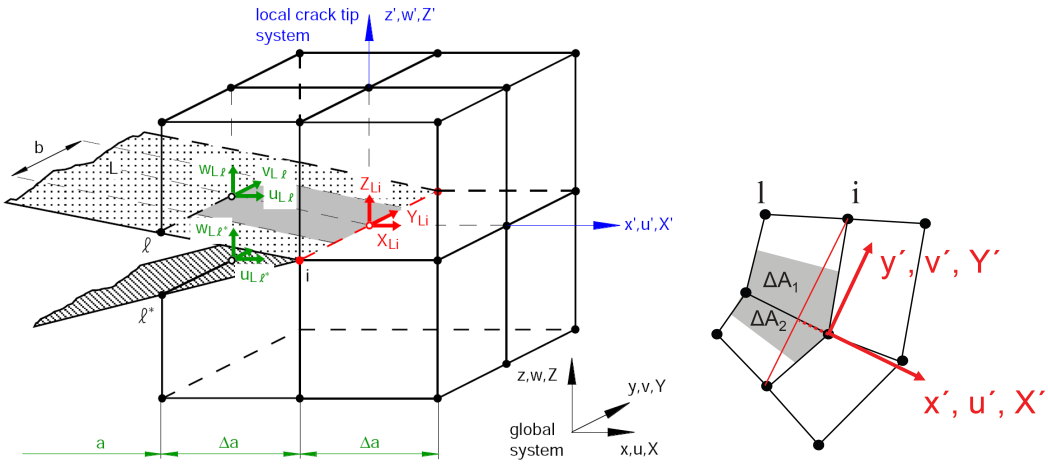

(a) 3D view [24]. (b) Top view.

Figure 7: Local crack tip configuration of an eight node solid element.

The energy release rates for the fracture mode components of the eight node solid element shown in figure 7 can be evaluated at the crack tip as follows:

$$G_I = -\frac{Z'_{Li}\left(w'_{Ll} - w'_{Ll^*}\right)}{2 \cdot (\Delta A_1 + \Delta A_2)} \quad , \quad G_{II} = -\frac{X'_{Li}\left(u'_{Ll} - u'_{Ll^*}\right)}{2 \cdot (\Delta A_1 + \Delta A_2)} \quad \text{and} \quad G_{III} = -\frac{Y'_{Li}\left(v'_{Ll} - v'_{Ll^*}\right)}{2 \cdot (\Delta A_1 + \Delta A_2)} \quad , \tag{4}$$

where X', Y' and Z' are the nodal forces transformed in the local coordinate system (x',y',z') of the crack tip and u', v' and w' the transformed displacements, respectively. Figure 7(b) shows the area definitions ΔA_1 and ΔA_2 as well as the definition of the local coodinate system for arbitrary shaped delamination contours.

5.2 The parametrized 3D model

The parametrized 3D delamination model presented in this work consists of the TBC system setup mentioned above. The basic setup of the implemented model consisting of a substrate and the thin layers of bond coat (BC) and top coat (TBC) is shown on the left of figure 8. The parametrized approach is modelled via the preprocessor ABAQUS/CAE. The initial delamination is idealized by the ellipse equation. The special case of a circle can also be chosen as can be seen on the left of figure 8. For this work 8 node linear solid elements are chosen for the complete model.

In case of ideal structures the local buckle phanomenon of the sublaminates can cause numerical solution difficulties. In order to countervail this effect a small imperfection can be introduced in the area of delamination, which may also be seen as a realistic effect caused by oxides. The out-of-plane global coordinates inside the delamination area are superimposed with a half cosine wave parallel to the local ξ, η coordinate system:

$$\Delta x_3 = h_i \cos\left(\frac{\pi}{2a}\xi\right)\cos\left(\frac{\pi}{2\bar{b}}\eta\right), \quad \bar{b} = b\sqrt{1 - \frac{\xi^2}{a^2}} \quad \text{within} \left(\frac{\xi}{a}\right)^2 + \left(\frac{\eta}{b}\right)^2 < 1, \tag{5}$$

where h_i is the maximal imperfection, and a and b are the major and minor semiaxes. This expression assures a tangential plane at the crack front between the intact TBC system and the delamination itself.

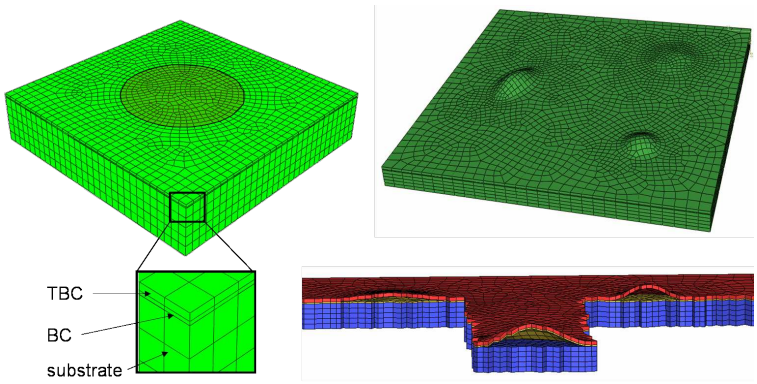

Figure 8: 3D delamination model

Futhermore, the parametrized model features variation in delamination position and orientation according to the global specimen. Multiple delaminations with individual interface positions substrate – BC or BC – TBC are possible as displayed on the right-hand side of figure 8. Elliptic representation in parametric coordinates allows for automatic spatial discretization enhancement in areas of large curvature.

5.3 Numerical results

In order to get first insights in the local loading conditions of TBC systems, sensitivities of initial delaminations are analysed. For the finite element analyses of the local approach displacement boundary conditions are extracted from the global model and applied to the local model as can be seen in figure 9.

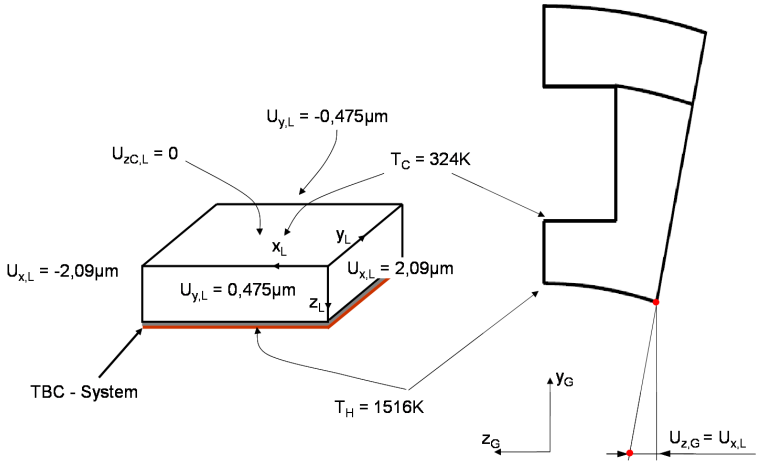

Figure 9: Transfer of boundary conditions from global to local model (BC = 30μm; TBC = 10μm).

The width of the local model is defined by one cooling channel at the nozzle throat region of the combustion chamber. The temperature boundary conditions of the copper substrate side are taken from position 2 of figure 5 and from position 4 at the hot wall for the top coat side, respectively. For simplicity to gain first insights, constant temperature and displacement boundary conditions are extracted and applied to the local model. The contraction displacement component $U_{z,G}$ of the chamber wall is extracted at the nozzle throat and applied symmetric for a full cooling channel as $U_{x,L}$ on the local model, which is shown in figure 9. In addition axial contraction of the thrust chamber is extracted for a small segment and applied likewise (see length and with in table 2).

The failure interface to be analysed in this study lies between the copper substrate and the bond coat material. This position was identified in experiments to be prone to failure mechanisms [26, 27]. In this study size variations of delamination circles are analysed for the above mentioned TBC systems. The delaminations are positioned in the

Table 2: Dimensions and boundary conditions applied to the local finite element model.

	BC = 30μm; TBC = 10μm	**BC = 100μm**
length / m	0.00168	0.00096
width / m	0.00198	0.00198
T_{TBC} / K	1516	1648
T_{SUB} / K	324	298
$U_{x,L}$ / m	±2.09e-06	±2.21e-06
$U_{y,L}$ / m	±4.75e-07	±2.85e-07

center of the interface plane of the local model. The copper substrate thickness at the nozzle throat is 1mm and the local maximum imperfection hight is defined with $h_i = 2\mu$m.

ABAQUS/Standard is used to solve the sequentially coupled thermomechanical finite element problem. Pre-analyses have shown that an element number of 320 along the crack front region is sufficient for the fracture mechanical post processing approach. The strainless condition is assumed at 293.15K, which is a first estimate and needs to be investigated in more detail in future studies.

Results of the fracture mode components G_{II} and G_{III} are shown in diagram 10. The fracture mode component G_I magnitude is about fourty times lower than the G_{II} and G_{III} components, consequently the loading condition does not result in a considerable opening of the delaminations in mode I direction. Sliding shear in mode II direction and scissoring shear in mode III direction are approximately in equal measure responsible for the failure mechanisms identified in the present sensitivity analyses. As expected the energy release rates start to elevate by increasing the delamination radius. A 10% increased delamination radius results rougly in a 25% increase of the energy release rate likewise for G_{II} and G_{III}.

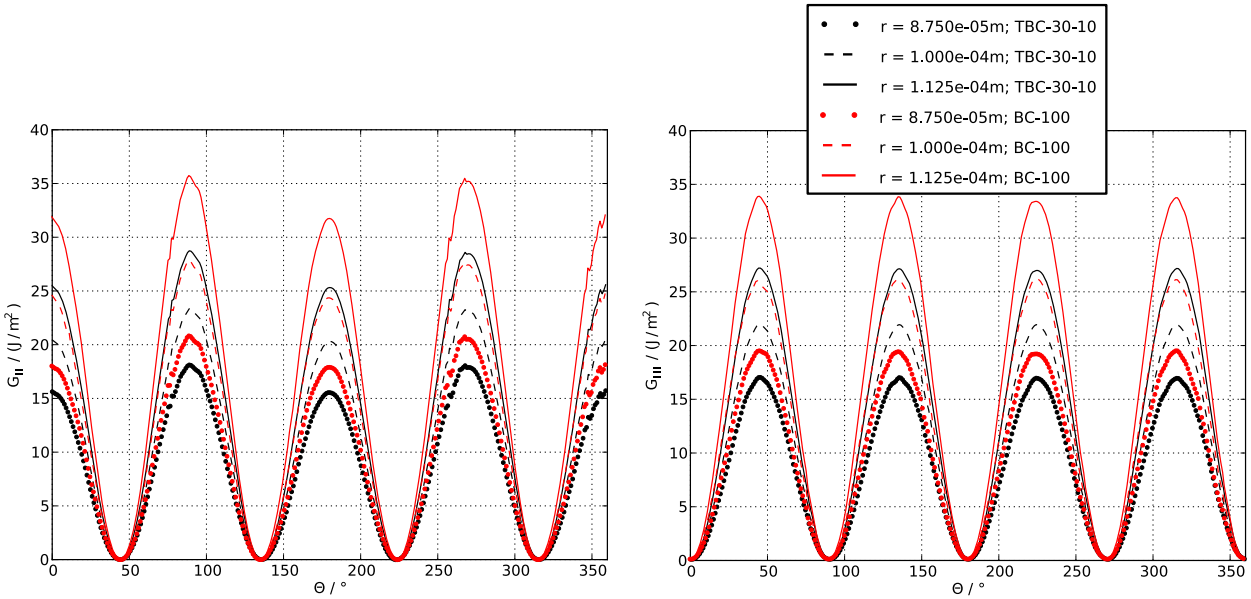

Figure 10: G_{II} and G_{III} vs Θ for two TBC systems and three delamination radii.

Comparing the two different TBC systems shown in diagram 10 one can conclude that the defined one layer bond coat setup is more critical towards delamination growth compared to the two layer TBC system setup.

6. Conclusions and outlook

A global full parametric 3D modelling approach for cooled rocket thrust chambers has been presented. Thermal and mechanical interactions have been analysed for the steady state case of a subscale thrust chamber taking into account

two different TBC systems. It was shown by global FSI analyses that one layer thermal protection systems are able to achieve the same protection as conventional two layer TBC systems.

Extracted boundary conditions of the global FSI analyses have been applied to a local finite element model to analyse possibe TBC delaminations, which have been investigated by a Fracture Mechanics approach. The fracture mode components II and III are identified to have the main influence on the failure mechanisms.

In the ongoing research the cooling fluid domains analysed by RANS model will be integrated in the presented fully coupled approach. Furthermore, transient effects will be investigated to address critical loading conditions for applied TBC systems. Thermal transient effects have a great impact on failure mechanisms of TBC systems. Future studies will focus on the application of transient loads and linear variation of boundary conditions applied to the local delamination model.

Acknowledgments

Financial support has been provided by the German Science Foundation (Deutsche Forschungsgemeinschaft - DFG) in the framework of the Collaborative Research Centre Transregio 40 TP D2 and D3. The authors would like to thank Astrium Space Transportation GmbH, Propulsion & Equipment for defining the subscale thrust chamber, which was studied in the present work.

References

[1] Kuhl, D., A. Woschnak, and O.J. Haidn. 1998. Coupled heat transfer and stress analysis of rocket combustion chambers. *34th AIAA/ASME/SAE/ASEE Joint Propulsion Conference, AIAA* 1998–3373.

[2] Fischer, S.C., M. Popp and R.J. Quentmeyer. 1995. Thrust Chamber Cooling and Heat Transfer. *2nd International Symposium on Liquid Rocket Propulsion*.

[3] Kuhl, D., J.R. Riccius, and O.J. Haidn. 2000. Thermomechanical Fluid-structure Analysis and Mathermatical Optimization Techniques Applied to Cryogenic Liquid Rocket Engine Design. *International Symposium on Liquid Space Propulsion.*

[4] Liu, Q.Y., E.A. Luke, and P. Cinella. 2005. Coupling Heat Transfer and Fluid Flow Solvers for Multidisciplinary Simulations. *Journal of Thermophysics and Heat Transfer* **19**(4), 417–427.

[5] Knab, O., M. Frey, J. Görgen, C. Maeding, K. Quering, and D. Wiedmann. 2009. Progress in Combustion and Heat Transfer Modelling in Rocket Thrust Chamber Applied Engineering. *45th AIAA/ASME/SAE/ASEE Joint Propulsion Conference, AIAA* 2009–5477.

[6] Haupt, M.C., R. Niesner, and R. Unger. 2006. Computational Aero-Structural Coupling for Hypersonic Applications. *9th AIAA/ASME Joint Thermophysics and Heat Transfer Conference, AIAA* 2006–3252.

[7] Haupt, M.C., R. Niesner, R. Unger and P. Horst. 2008. Numerical Analysis of Thin-Walled Structures in Hypersonic Flow Regime. *ICAS 2008 Congress*.

[8] Haupt, M.C., R. Niesner, P. Horst, B. Esser and A. Gülhan. 2009. Computational Analysis of a Heat Transfer Experiment Including Thermally Induced Deformations. *First Int. Conference on Comp. Meth. for Thermal Problems (ThermaComp2009)*.

[9] Park, K., and C. Felippa. 2000. A Variational Principle for the Formulations of Partitioned Structural Systems. *Int. J. Numer. Meth. Engng.* **47**, 395–418.

[10] Unger, R., M.C. Haupt and P. Horst. 2007. Application of Lagrange Multipliers for Coupled Problems in Fluid and Structural Interactions. *Computers & Structures* **85**, 796–809.

[11] Shewchuk, J., R. 2002. Delaunay refinement algorithms for triangular mesh generation. *Computational Geometry: Theory and Applications* **22**(1-3), 21–74.

[12] Si, H. 2006. TetGen: A quality tetrahedral mesh generator and a 3d delaunay triangulator. *http://tetgen.berlios.de*.

[13] Rao, G.V.R. 1958. Exhaust Nozzle Contour for Optimum Thrust. *Jet Propulsion* **28**, 377–382.

[14] Östlund, J. 2002. Flow processes in rocket engine nozzles with focus on flow separation and side-loads. *Licentiate Thesis, Royal Institute of Technology, Department of Mechanics, Stockholm*.

[15] Ponomarenko, A. 2009. RPA: Design Tool for Liquid Rocket Engine Analysis. *http://www.lpre.de/resources/software/RPA_en.htm*

[16] TAU-Code DLR. 2009. Technical Documentation of the DLR TAU-Code. *Institut of Aerodynamics and Flow Technology Braunschweig*

[17] Deutsches Kupferinstitut. 2005. Kupferdatenblatt CuCr1Zr.

[18] Freborg, A.M., B.L. Ferguson, W.J. Brindley, and G.J. Petrus. 1998. Modeling oxidation induced stresses in thermal barrier coatings. *Materials Science and Engineering* **245**, 182–190.

[19] Esposito, J.J., and R.F. Zabora. 1997. "'Thrust Chamber Life Prediction"' Volume I - Mechanical and Physical Properties of High Performance Rocket Nozzle Materials. *NASA Report* NASA CR–134806.

[20] Special Metals. 2008. INCONEL alloy 600. *http://www.specialmetals.com/products/inconelalloy600.php*

[21] Quentmeyer, R.J. 1977. Experimental Fatigue Life Investigation of Cylindrical Thrust Chambers. *AIAA* 77–893.

[22] Miller, R.A., and C.E. Lowell, C.E. 1982. Failure Mechanisms of Thermal Barrier Coatings Exposed to Elevated Temperatures. *Thin Solid Films* **95**, 265–273.

[23] Rice, J.R. 1968. A path independent integral and the approximate analysis of strain concentration by notches and cracks. *J. App. Mech.* **68**, 379–386.

[24] Krueger, R. 2002. Virtual Crack Closure Technique: history, approach, and applications. *Appl. Mech. Rev.* **57**, 109–143.

[25] Williams, J.G. 1988. On the calculation of energy release rates for cracked laminates. *Int. J. Frac.* **36**, 101–119.

[26] Schloesser, J., D. Kowollik, M. Bäker, J. Rösler and P. Horst. 2010. Failure analysis and multiscale modeling of thermal barrier coatings. *SFB/TRR 40 Annual Report 2010*. Institute of Aerodynamics and Fluid Mechanics.

[27] Schloesser, J., M. Bäker, J. Rösler and R. Pulz. 2010. Oxidation Behavior of Thermal Barrier Coatings on Copper Substrates. *Advances in Science and Technology* **66**, 74–79.